Photocurrent analysis of quantum cascade detectors by magnetotransport

François-Régis Jasnot,[1] Nicolas Péré-Laperne,[1] Louis-Anne de Vaulchier,[1,][*] Yves Guldner,[1] Francesca Carosella,[1] Robson Ferreira,[1] Amandine Buffaz,[2] Laetitia Doyennette,[2] Vincent Berger,[2] Mathieu Carras,[3] and Xavier Marcadet[3]

[1]*Laboratoire Pierre Aigrain, Ecole Normale Supérieure, CNRS UMR 8551, Université P. et M. Curie–Université Paris Diderot, 24 rue Lhomond, 75231 Paris Cedex 05, France*

[2]*Laboratoire Matériaux et Phénomènes Quantiques, Université Paris Diderot—Paris 7, CNRS-UMR 7162, Bâtiment Condorcet, 75205 Paris Cedex 13, France*

[3]*Alcatel-Thales 3-5 lab, Route départementale 128, 91767 Palaiseau Cedex, France*
(Received 7 May 2010; revised manuscript received 22 July 2010; published 27 September 2010)

Photocurrent measurements have been performed on a quantum cascade detector structure under strong magnetic field B applied parallel to the growth axis. The photocurrent shows oscillations as a function of B. In order to describe this behavior, we have developed a rate equation model. The interpretation of the experimental data supports the idea that an elastic scattering contribution plays a central role in the behavior of these structures. We present a calculation of the electron lifetime versus magnetic field which suggests that impurities scattering in the active region is the limiting factor. These experiments lead to a better understanding of these complex structures and identify key parameters to optimize them further.

I. INTRODUCTION

The quantum cascade detector,[1] (QCD) recently proposed and realized in both the midinfrared[2] and in the terahertz[3,4] range, is a photovoltaic version of the quantum well infrared photodetector (QWIP).[5] The band structure of these devices is designed as a quantum cascade laser (QCL) under no applied electric field.[1,3] As such, the QCD structure is designed to generate an electronic displacement under illumination through a cascade of quantum levels without the need of an applied voltage. They are totally passive systems and show a response only to photon excitation. Owing to this photovoltaic behavior, QCDs can work with a higher doping level than QWIPs and therefore possess higher quantum efficiencies (QEs), lower dark currents, and longer integration times.

QCDs have already been realized with different material systems over the last few years.[2,6–8] A typical midinfrared QCD structure contains several identical periods, each one of them containing between five and ten coupled quantum wells. A period is made of an "active region" dedicated to the absorption of infrared photons and a "cascade region" optimized for the electron transfer between two consecutive regions.

In a semiconductor quantum well structure, a magnetic field applied along the growth direction breaks the two-dimensional in-plane continuum into discrete Landau levels (LLs). This experimental technique has been used to evaluate the different contributions of various scattering mechanisms in complex quantum cascade structures.[4,9–12] The aim of the current magnetophotocurrent study is to understand electronic transport in QCDs under illumination and to study the scattering mechanisms involved in these complex structures at their working temperature (80 K). We further develop a simple model of transport under illumination in a QCD as well as calculations of rates for various electron scattering mechanisms. Through a comparison between experimental and calculation results, we highlight the mechanism limiting the response of QCDs.

II. QCD STRUCTURE

The QCD under study is a GaAs/AlGaAs heterostructure with a detection wavelength of 8 μm. It consists of 40 identical periods of seven coupled GaAs quantum wells (QWs). $Al_{0.34}Ga_{0.66}As$ barriers are used in order to reach a conduction band offset of 275 meV. N doping of the first QW (5 $\times 10^{11}$ cm^{-2}) of each period allows to populate its first energy level |down⟩ in the conduction band with electrons (see Fig. 1). We stress the fact that such doping level is much higher than in standard QCL structures and also that dopants are placed in the first QW, i.e., in the active region of the QCD. The layer sequence in Å starting from the first quantum well is as follows 67.8/**56.6**/19.8/**39.6**/22.6/**31.1**/28.3/ **31.1**/33.9/**31.1**/39.6/**31.1**/45.2/**50.8** (the barrier widths are represented in bold types).

Figure 1 recalls the principle of the device: owing to the absorption of a midinfrared photon, an electron is excited
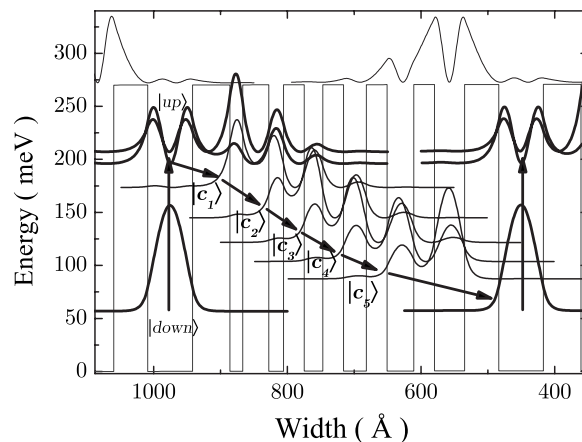

FIG. 1. Conduction band diagram of one period of an 8 μm QCD showing the wave function of each energy levels. Note that the ground state of the first QW belongs to the former period and is noted |down⟩. The arrows illustrate the electronic path during a detection event.
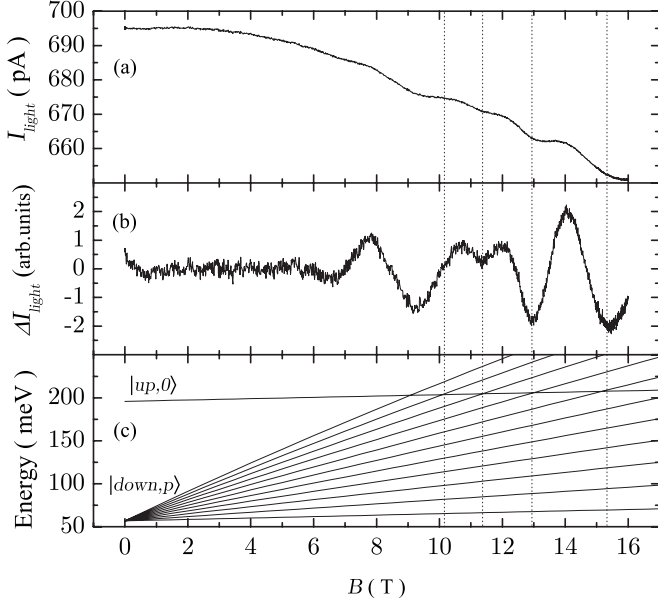
FIG. 2. (a) Current under illumination as a function of magnetic field at zero bias. (b) I_{light} as a function of the magnetic field where the contribution of the magnetoresistance has been subtracted. (c) Fan chart of $|up,0\rangle$ and $|down,p\rangle$ as a function of B from Eq. (1) taking into account the band nonparabolicity.

from the fundamental level of the structure $|down\rangle$ to the upper levels $|up\rangle$ which are delocalized across the first two QWs. High dipole matrix elements between $|up\rangle$ and the other energy levels of the cascade allows electrons to be transferred to the right QWs as a result of a series of LO-phonon scattering events. Levels in the cascade are labeled $|c_i\rangle$ with $i=1-5$. The last QW of the cascade is identical to the first one and the period is repeated in order to increase the induced potential that results from this electron transfer. By closing the circuit, a significant photocurrent is expected without any applied bias. The studied samples are 100 $\times 100$ μm^2 square mesas obtained by reactive ion etching.

III. MAGNETOPHOTOCURRENT MEASUREMENTS

QCDs are mounted inside an insert at the center of a superconducting coil where a magnetic field B up to 16 T can be applied parallel to the growth axis. Light is emitted by a globar source from a Fourier transform infrared spectrometer and guided to the sample. The experiment consists in measuring the current under illumination I_{light}, without any applied voltage, at 80 K while the magnetic field is swept from zero to its maximum value.

Typical results are shown in Fig. 2(a). The photocurrent shows oscillations as a function of the magnetic field, superposed on a general behavior corresponding approximately to a quadratic decrease. This main decreasing component is attributed to the magnetoresistance of the contacts of the sample.[12] This quadratic decrease has been removed from the experimental data in Fig. 2(b).

At zero magnetic field, all the quantum levels of a period have plane-wavelike energy dispersion in the direction par-

allel to the layers. At 0 V and without any illumination, electronic transitions from one level to another compensate each other resulting in zero current (the system is in equilibrium).[13] When a magnetic field is applied along the growth axis, the subbands split into ladders of discrete Landau levels given by

$$E_{n,p} = E_n^0 + \left(p + \frac{1}{2}\right)\hbar\omega_c, \qquad (1)$$

where n and p are integers, n is the index of the subband and p the index of the Landau level, $\hbar\omega_c=\hbar eB/m^\star$ is the cyclotron energy, e is the electronic charge and $m^\star$ the effective mass in GaAs. E_n^0 is the energy of the subband edge at zero magnetic field. The effect of the magnetic field on the QCD photocurrent is quite similar to that in a three-level active region of a QCL where electron scattering from the upper state is modulated by the magnetic field.[9,10] Indeed, depending on the value of the magnetic field, the Landau level arrangement strongly influences the scattering of electrons from the various $|up,0\rangle$ levels to $|n,p\rangle$, where $|n,p\rangle$ designates the p Landau level originating from subband n.

Figure 2(c) represents the evolution in energy of the Landau levels $|up,0\rangle$ and $|down,p\rangle$ as a function of magnetic field from Eq. (1), taking into account the band nonparabolicity. Minima of current in magnetic field are in good agreement with crossing of LL $|up,0\rangle$ with LLs $|down,p\rangle$ with $p=6,7,8,9$ at $B=15.3$ T, 13.0 T, 11.4 T, and 10.1 T, respectively (dashed vertical bars in Fig. 2). Comparing Figs. 2(b) and 2(c) leads to the conclusion that an elastic scattering mechanism is dominant in this structure and mainly involves $|up\rangle$ and $|down\rangle$ levels. A complete description of the mechanisms involved in the photocurrent and a model describing it as a function of B are presented in Secs. IV and V. Oscillations at low magnetic field, between $B=4$ and 9 T are described in Sec. V.

IV. MODEL AND SCATTERING MECHANISMS INVOLVED IN THE CURRENT

In a previous paper, we presented magnetocurrent measurement without any illumination.[12] These experiments put in evidence some leakages from level $|down\rangle$ to the levels in the next cascade when the detector is submitted to an applied bias. This current is called the dark current (I_{dark}) and we demonstrated I_{dark} originates from several parallel cross transitions for a fixed temperature. As described in Sec. III, we do not apply any bias on our structure for these photocurrent experiments: the current measured in this work originates from a displacement of electrons after a photon absorption.

In this part, we describe in detail the model that leads to the magnetophotocurrent oscillations in a QCD. We propose a model of transport within one single period by a rate equation approach. We assume that electrons are in the upper detector state ($|up\rangle$) through absorption of a photon and we establish the rate equation for this level. Electrons can leave this state either by falling back to the fundamental level $|down\rangle$ or through the cascade $|c_i\rangle$. i.e.,

TABLE I. Scattering rates in s^{-1} are calculated using different scattering processes for an electron in the $|$up$\rangle$ subband at $B=0$ T.

Scattering mechanism	$1/\tau_{\text{up-down}}$	$1/\tau_{\text{up-}c}$
LO phonon emission	7.0×10^{11}	7.9×10^{11}
Interface roughness	6.0×10^{11}	8.6×10^{12}
Impurity scattering	1.8×10^{13}	5.2×10^{13}

$$\frac{dN_{\text{up}}}{dt} = \frac{N_{\text{down}}}{\tau_{\text{down-up}}} - \frac{N_{\text{up}}}{\tau_{\text{up-down}}} + \frac{N_c}{\tau_{c\text{-up}}} - \frac{N_{\text{up}}}{\tau_{\text{up-}c}} + \alpha N_{\text{down}}, \quad (2)$$

where the subscribe c stands for the whole cascade, N_i is the sheet density of level $|i\rangle$, $\frac{1}{\tau_{\text{up-}c}}=\Sigma_{i=1}^5\frac{1}{\tau_{\text{up-}c_i}}$, τ_{m-n} the scattering time of an electron in level $|m\rangle$ toward the level $|n\rangle$ and α the absorption efficiency coefficient. The current we are measuring in our macroscopic experimental setup is given by

$$\frac{J}{q} = \frac{N_{\text{up}}}{\tau_{\text{up-}c}} - \frac{N_c}{\tau_{c\text{-up}}}, \quad (3)$$

where J is the current density and q the charge of electron. We recall the equilibrium conditions explained in Sec. III when no bias is applied and without illumination

$$\begin{cases} \dfrac{N_{\text{down}}^e}{\tau_{\text{down-up}}} = \dfrac{N_{\text{up}}^e}{\tau_{\text{up-down}}} \\[2mm] \dfrac{N_{\text{up}}^e}{\tau_{\text{up-}c}} = \dfrac{N_c^e}{\tau_{c\text{-up}}}. \end{cases} \quad (4)$$

The exponent "e" signifies equilibrium. We assume that the population of level $|$down$\rangle$ is the same in equilibrium and under illumination ($N_{\text{down}}\approx N_{\text{down}}^e$) and obviously the population of level $|$up$\rangle$ varies under illumination ($N_{\text{up}}\neq N_{\text{up}}^e$).

In a stationary state we find from Eqs. (2) and (3)

$$\frac{J}{q} = \frac{N_{\text{up}}^e}{\tau_{\text{up-down}}} - \frac{N_{\text{up}}}{\tau_{\text{up-down}}} + \alpha N_{\text{down}}. \quad (5)$$

The variation in population of level $|$up$\rangle$ in the two different situations can be expressed as

$$N_{\text{up}} - N_{\text{up}}^e = \alpha N_{\text{down}}\tau_{\text{up}}, \quad (6)$$

where $\frac{1}{\tau_{\text{up}}} = \frac{1}{\tau_{\text{up-down}}} + \frac{1}{\tau_{\text{up-}c}}$.

As a conclusion the current is given by

$$\frac{J}{q} = \alpha N_{\text{down}}\left(\frac{\tau_{\text{up-down}}}{\tau_{\text{up-down}} + \tau_{\text{up-}c}}\right) = \alpha N_{\text{down}}\text{QE}. \quad (7)$$

As mentioned above, as α and N_{down} are constant, the only figure which varies under magnetic field is the QE, as a function of the subband lifetimes.

This model is in agreement with the trade-off presented in Ref. 12, where the efficiency of the detector is ruled by the ability to generate photocarriers and then to extract them owing to the cascade. As a consequence, both lifetimes $\tau_{\text{up-down}}$ and $\tau_{\text{up-}c}$ have to be involved in the photocurrent.

The lifetimes are directly obtained from calculation of the scattering rates of the different elastic and inelastic mecha-

nisms. As mentioned in Refs. 10 and 14, two mechanisms are dominant in these midinfrared GaAs cascade structures—LO-phonon emission and interface roughness.

We present in Table I the calculated scattering rates of the different processes at $B=0$ T. For interface roughness, we used a Gaussian autocorrelation of the roughness with an average height of $\Delta=2.8$ Å and a correlation length of $\Lambda=60$ Å.[15] LO-phonon emission scattering time has been calculated as in Ref. 14. In our structure, a third scattering mechanism becomes important—ionized impurities scattering. In Ref. 10 this process has been neglected as the doped layers were separated from the optical transition. In this work, instead, the doping level is much higher and the doped layers is in the core of the active region. As a direct consequence of these two effects, we calculate that impurities scattering is the most efficient process in our system.

In order to take into account the main scattering process we calculate ionized-impurities scattering as a function of magnetic field. The electron-ionized impurity interaction potential is given by[16]

$$V_{\text{imp}}(\mathbf{R}, \mathbf{R}_i) = \frac{2\pi e^2}{4\pi\varepsilon_0\varepsilon_r S}\sum_{\mathbf{Q}_\perp}\frac{1}{Q_\perp}\exp[-Q_\perp|z-z_i|$$
$$+ i\mathbf{Q}_\perp\cdot(\boldsymbol{\rho}-\boldsymbol{\rho}_i)], \quad (8)$$

where $S=L_xL_y$ is the sample surface, $\mathbf{R}_i=(\boldsymbol{\rho}_i,z_i)$ is the impurity position in the well, and $\mathbf{Q}_\perp=(Q_x,Q_y)$ is the electron wave vector in the layer plane. The electron wave function, in presence of a magnetic field applied along the heterostructure growth direction, is given by

$$|m,n,k_y\rangle = \chi_m(z)\phi_n(x+\ell_c^2k_y)\frac{e^{ik_yy}}{\sqrt{L_y}}, \quad (9)$$

where $\chi_m(z)$ is the heterostructure envelope function corresponding to the mth subband, ϕ_n is the nth Hermite function associated with the nth Landau level, and $\ell_c=\sqrt{\hbar/eB}$ is the magnetic length. We calculate the scattering time for an electron in the lowest Landau level ($n=0$) of the upper subband toward the Landau levels of lower subband using Fermi's golden rule and assuming broadened Landau levels,[14] giving

$$\left\langle\frac{1}{\tau_{2,n=0,k_y}}\right\rangle = \frac{2\pi}{\hbar}\sum_i\sum_{n'}\sum_{k_y'}|\langle 1,n',k_y'|V_{\text{imp}}(\mathbf{R},\mathbf{R}_i)$$
$$\times|2,n=0,k_y\rangle|^2\frac{1}{\delta\sqrt{2\pi}}$$
$$\times\exp\left[-\frac{(E_2-E_1-n'\hbar\omega_c)^2}{2\delta^2}\right], \quad (10)$$

where δ is the broadening parameter of LLs. According to Ref. 14, the inhomogeneous broadening model results in an expression of the average scattering rate which resembles that obtained by replacing the deltalike peaks of the Landau levels density of states by Gaussian functions. As such we take $\delta=6$ meV, a value consistent with $\hbar/\tau_{\text{up-down}}^{imp}$ obtained in the following. The calculation of the matrix element leads to

$$\left\langle \frac{1}{\tau_{2,n=0,k_y}} \right\rangle = \frac{2\pi}{\hbar} \left(\frac{e^2}{4\pi\varepsilon_0\varepsilon_r} \right)^2 N_{\text{imp}_S}$$

$$\times \sum_{z_i} \sum_{n'} \int\int \frac{dQ_x dQ_y}{Q_x^2 + Q_y^2} |\langle 1| e^{-\sqrt{Q_x^2 + Q_y^2}|z-z_i|}$$

$$\times |2\rangle|^2 |\langle n', k_y + Q_y | e^{iQ_x x} | n = 0, k_y \rangle|^2$$

$$\times \frac{1}{\delta\sqrt{2\pi}} \exp\left[-\frac{(E_2 - E_1 - n'\hbar\omega_c)^2}{2\delta^2} \right],$$

where N_{imp_S} is the area impurity density. Making the variable change $\tilde{x} = x + \ell_c^2 k_y$ and following Mycielski *et al.*[17] we obtain

$$\langle n', k_y + Q_y | e^{iQ_x x} | n = 0, k_y \rangle = e^{-iQ_x \ell_c^2 k_y} \frac{1}{\sqrt{n'!}} \exp\left(-\frac{i}{2} \ell_c^2 Q_x Q_y \right)$$

$$\times \left(\frac{\ell_c}{\sqrt{2}} \right)^{n'} (Q_y + iQ_x)^{n'}$$

$$\times \exp\left[-\frac{1}{4} \ell_c^2 (Q_x^2 + Q_y^2) \right], \quad (11)$$

which introduced in the previous equation gives

$$\left\langle \frac{1}{\tau_{2,n=0,k_y}} \right\rangle = \frac{2\pi}{\hbar} \left(\frac{e^2}{4\pi\varepsilon_0\varepsilon_r} \right)^2 N_{\text{imp}_S}$$

$$\times \sum_{z_i} \sum_{n'} \frac{1}{n'!} \left(\frac{\ell_c^2}{2} \right)^{n'} \int\int dQ_x dQ_y (Q_x^2$$

$$+ Q_y^2)^{n'-1} \exp\left[-\frac{\ell_c^2}{2} (Q_x^2 + Q_y^2) \right] |\langle 1| e^{-\sqrt{Q_x^2 + Q_y^2}|z-z_i|}$$

$$\times |2\rangle|^2 \frac{1}{\delta\sqrt{2\pi}} \exp\left[-\frac{(E_2 - E_1 - n'\hbar\omega_c)^2}{2\delta^2} \right]. \quad (12)$$

Then using polar coordinates $dQ_x dQ_y = Q_\perp dQ_\perp d\theta$ and making the variable change $X = \frac{\ell_c^2}{2} Q_\perp^2$, the final expression obtained is

$$\left\langle \frac{1}{\tau_{2,n=0,k_y}} \right\rangle = \frac{2\pi^2}{\hbar} \left(\frac{e^2}{4\pi\varepsilon_0\varepsilon_r} \right)^2 N_{\text{imp}_S} \sum_{z_i} \sum_{n'} \frac{1}{\delta\sqrt{2\pi}}$$

$$\times \exp\left[-\frac{(E_2 - E_1 - n'\hbar\omega_c)^2}{2\delta^2} \right] \frac{1}{n'!}$$

$$\times \int_0^{+\infty} X^{n'-1} e^{-X} \left| \langle 1| \exp\left(-\frac{\sqrt{2X}}{\ell_c} |z - z_i| \right) \right.$$

$$\left. \times |2\rangle \right|^2 dX.$$

Figure 3 presents a comparison between the experimental data and the calculated electron-ionized impurities scattering times as a function of magnetic field. Minima in photocurrent at high field correspond to minima in the calculation (vertical dotted lines) and the photocurrent behavior is attributed to oscillations of $\tau_{\text{up-down}}^{imp}$.
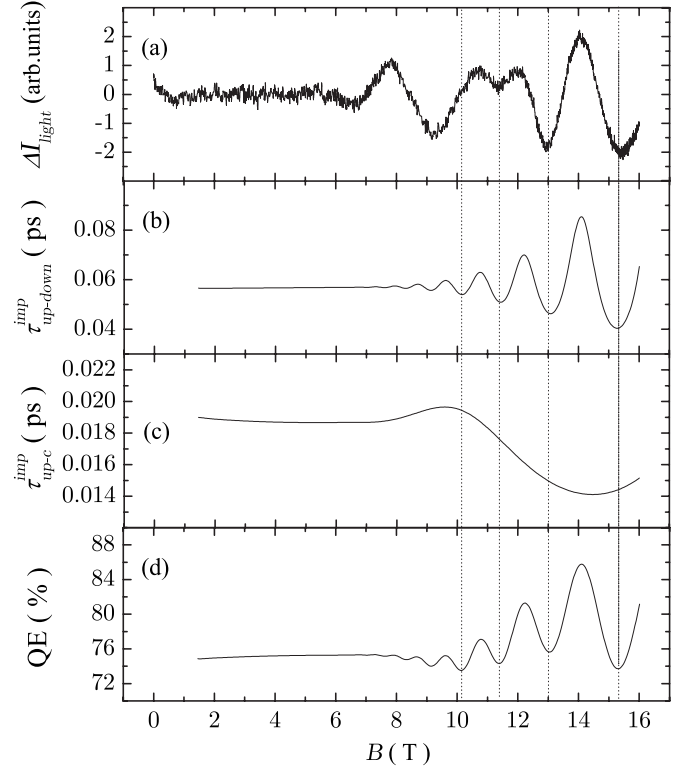

FIG. 3. (a) ΔI_{light} as a function of magnetic field where the contribution of the magneto-resistance has been subtracted (Ref. 12). (b) Ionized impurity scattering $\tau_{\text{up-down}}^{imp}$ under magnetic field between |up⟩ and |down⟩ levels. (c) Ionized impurity scattering $\tau_{\text{up-c}}^{imp}$ under magnetic field between |up⟩ and levels in the cascade. (d) QE calculated with Eq. (7).

V. INTERPRETATION OF EXPERIMENTAL DATA

In this section, we concentrate on the description of photocurrent as a function of B owing to Eq. (7). Low magnetic field photocurrent oscillations are also discussed. Figure 3 presents a comparison between experimental results and our model. Figures 3(b) and 3(c) show the two scattering times involved in Eq. (7) as a function of B calculated with electron-ionized impurities scattering. Figure 3(d) shows the calculation of the related quantum efficiency.

First, the oscillating behavior at high magnetic field ($B > 9$ T) originates from the scattering process involved in the electronic transfer from |up⟩ to |down⟩. This transfer leads to minima in the current which fit well with $\tau_{\text{up-down}}^{imp}$ and the QE. At the same time $\tau_{\text{up-c}}^{imp}$ has a long period oscillating behavior as a function of B enhancing the peak in QE at $B = 14$ T in accordance with experimental data. QE is the most relevant figure and describes the performance of the detector. Under magnetic field, the QE oscillates between 74% and 85%. Note that, on one hand, ionized impurities scattering is a limiting factor within $\tau_{\text{up-down}}^{imp}$ but, on the other hand, is an enhancing factor for $\tau_{\text{up-c}}^{imp}$. By extrapolating the data under magnetic field, at $B = 0$ T, QE is equal to 75%, a value that should be increased to improve the detector performance. An optimized structure should take these results into account by shifting the ionized impurities from the active region, where they are enhancing $1/\tau_{\text{up-down}}^{imp}$, to a position where they would only contribute to $\tau_{\text{up-c}}^{imp}$.

Second, at low magnetic field ($B < 9$ T), there is a discrepancy between the experimental oscillating behavior and the calculate QE, especially at 8 T where the data show a broad peak. There can be two reasons for this: (i) the calculation of $\tau_{up\text{-}c}$ itself or (ii) a scattering mechanism for the transport of electrons away from the active region, inside the cascade. Concerning the first one, in the calculation of $\tau_{up\text{-}c}$ we took into account the impurity scattering mechanism which is found to be stronger than any other mechanism, in particular, LO-phonon emission. This is due to the fact that the energy separation between the $|up\rangle$ and $|c_1\rangle$ states is short by ~ 13 meV to the LO-phonon energy. But there exists a particular magnetic field at which the first Laudau level of $|up\rangle$ will be separated from $|c_1\rangle$ by exactly one LO phonon. This should occur at $13/1.6 \approx 8$ T and would enhance greatly the extraction of electrons from the active region to the cascade. Concerning the second mechanism that can enhance the peak at 8 T, it can be seen in Fig. 2(b) that ΔI_{light} presents actually two maxima at $B = 5.8$ T and $B = 8$ T. According to Eq. (1), the characteristic energy of this series of oscillations is $\Delta E \sim 37$ meV. This energy is close to the separation energy of subsequent levels in the cascade. In the vicinity of the crossings of $|c_i, 0\rangle$ and $|c_{i+1}, p\rangle$, interface roughness scattering enhances the flow of electrons through the cascade. Assuming that this series is relevant for our structure, two extra maxima should arise at $B = 11.7$ T and $B = 23.4$ T. The latter is out of our experimental range, but the former is present on ΔI_{light} curve superimposed on the short period oscillating behavior of $\tau_{up\text{-}down}^{imp}$. As such, this new series of resonances in the cascade region also provides an explanation to the discrepancy in amplitude between the experimental results and the calculation of QE around 12 T.

Previously, two models were developed for this structure to describe the dark current.[12,18] The first one assumed a quasi-Fermi equilibrium on all the structure due to a fast extraction in the cascade whereas the second one assumed a thermalized population in each subband of the cascade. This second model helped to describe the dark current at high temperatures and pointed out the cascade design as a crucial step in the structure definition. Thanks to the present work, extraction toward the cascade as well as intracascade resonances are highlighted as optimizing factors which have to be improved to increase the performance of the detector.

Finally, it is worth stressing that the physics in this particular QCD is quite different from the one in usual quantum cascade structures (for example, quantum cascade lasers) because the doping level is much higher and positioned in the active absorption layer. As a consequence, usual scattering interactions are calculated to be less efficient than the impurity scattering as shown in Table I. For instance in Ref. 3, the doping level corresponds to an effective sheet carrier density of 8.7×10^9 cm^{-2} instead of 5×10^{11} cm^{-2} in our sample. As such, there is no contradiction with former work in quantum cascade structures.

VI. CONCLUSION

In conclusion, we have investigated the photocurrent in a midinfrared quantum cascade detector as a function of magnetic field. We have described the high magnetic field oscillations by an elastic scattering mechanism, namely electron-ionized impurities scattering, which is found to be the dominant scattering mechanism in our sample. We have also developed a model to describe the photocurrent in this structure. It highlights the trade-off in transport in this structure involving both a limiting scattering time $\tau_{up\text{-}down}^{imp}$ and an enhancing scattering time $\tau_{up\text{-}c}^{imp}$. We have performed calculations in order to describe electron-impurities scattering as a function of magnetic field and to evaluate $\tau_{up\text{-}down}^{imp}$ and $\tau_{up\text{-}c}^{imp}$. Finally, we have used both our model and calculations to define and evaluate the quantum efficiency of the structure. In order to improve further this efficiency, we suggest to shift the impurities in another location of the structure in order to minimize $1/\tau_{up\text{-}down}^{imp}$. Moreover magnetic field has allowed us to highlight the crucial part of the design of the cascade in order to enhance $\tau_{up\text{-}c}^{imp}$. Thanks to this work we assess the different fundamental electronic mechanisms within these complex heterostructures.

*louis-anne.devaulchier@lpa.ens.fr

[1] L. Gendron, M. Carras, A. Huynh, V. Ortiz, C. Koeniguer, and V. Berger, Appl. Phys. Lett. **85**, 2824 (2004).

[2] L. Gendron, C. Koeniguer, V. Berger, and X. Marcadet, Appl. Phys. Lett. **86**, 121116 (2005).

[3] M. Graf, G. Scalari, D. Hofstetter, J. Faist, H. Beere, E. Linfield, D. Ritchie, and G. Davies, Appl. Phys. Lett. **84**, 475 (2004).

[4] G. Scalari, M. Graf, D. Hofstetter, J. Faist, H. Beere, and D. Ritchie, Semicond. Sci. Technol. **21**, 1743 (2006).

[5] B. F. Levine, K. K. Choi, C. G. Bethea, J. Walker, and R. J. Malik, Appl. Phys. Lett. **50**, 1092 (1987).

[6] M. Graf, N. Hoyler, M. Giovannini, J. Faist, and D. Hofstetter, Appl. Phys. Lett. **88**, 241118 (2006).

[7] F. R. Giorgetta, E. Baumann, M. Graf, L. Ajili, N. Hoyler, M. Giovannini, J. Faist, and D. Hofstetter, Appl. Phys. Lett. **90**, 231111 (2007).

[8] A. Buffaz, M. Carras, L. Doyennette, A. Nedelcu, X. Marcadet, and V. Berger, Appl. Phys. Lett. **96**, 172101 (2010).

[9] D. Smirnov, O. Drachenko, J. Leotin, H. Page, C. Becker, C. Sirtori, V. Apalkov, and T. Chakraborty, Phys. Rev. B **66**, 125317 (2002).

[10] A. Leuliet, A. Vasanelli, A. Wade, G. Fedorov, D. Smirnov, G.

Bastard, and C. Sirtori, Phys. Rev. B **73**, 085311 (2006).

[11] N. Péré-Laperne, L. A. de Vaulchier, Y. Guldner, G. Bastard, G. Scalari, M. Giovannini, J. Faist, A. Vasanelli, S. Dhillon, and C. Sirtori, Appl. Phys. Lett. **91**, 062102 (2007).

[12] A. Gomez, N. Péré-Laperne, L. A. de Vaulchier, C. Koeniguer, A. Vasanelli, A. Nedelcu, X. Marcadet, Y. Guldner, and V. Berger, Phys. Rev. B **77**, 085307 (2008).

[13] C. Koeniguer, G. Dubois, A. Gomez, and V. Berger, Phys. Rev. B **74**, 235325 (2006).

[14] C. Becker, A. Vasanelli, C. Sirtori, and G. Bastard, Phys. Rev. B **69**, 115328 (2004).

[15] H. Sakaki, T. Noda, K. Hirakawa, M. Tanaka, and T. Matsusue, Appl. Phys. Lett. **51**, 1934 (1987).

[16] R. Ferreira and G. Bastard, Phys. Rev. B **40**, 1074 (1989).

[17] J. Mycielski, G. Bastard, and C. Rigaux, Phys. Rev. B **16**, 1675 (1977).

[18] A. Buffaz, A. Gomez, M. Carras, L. Doyennette, and V. Berger, Phys. Rev. B **81**, 075304 (2010).